Scene-based Cross-comparison of SNPP-VIIRS and Aqua-MODIS over Oceanic Waters

Nima Pahlevan*[a], Zhongping Lee[a], Adam Lawson[b] , Robert Arnone[c]

[a]School for the Environment, University of Massachusetts at Boston, Boston, MA 02125, USA
[b]Naval Research Lab, Stennis Space Center, MS 39529, USA
[c]Department of Marine Sciences, University of Southern Mississippi, Stennis Space Center, MS 39529,USA

ABSTRACT

The Visible Infrared Imaging Radiometer Suite (VIIRS) onboard the Suomi National Polar-orbiting Operational Environmental Satellite System (NPOESS) Preparatory Project (NPP) (SNPP) was launched in October 2011 to continue monitoring the globe in a similar fashion as the heritage sensors, such as the MODerate resolution Imaging Spectroradiometer (MODIS). This paper applies a scene-based technique to examine in-orbit radiometric stability of VIIRS relative to Aqua MODIS. The cross-comparison is made over global deep ocean waters. This cross-comparison allows for a comprehensive examination of the sensors' radiometric responsivity at relatively low signal levels (over oceanic waters). The study is further extended to L2/L3 products, including remote sensing reflectance and the inherent optical properties (IOPs) of waters under investigation, derived from the top-of-atmosphere (TOA) radiance (L1B). The temporal analyses give insights into the trends in the relative radiometric stability and the resulting discrepancies in the corresponding products.

Keywords: ocean color remote sensing, temporal consistency, VIIRS, MODISA

1. INTRODUCTION

Multi-decade, continuous, and reliable ocean color (OC) products require careful radiometric inter-comparisons among various OC sensors. This ensures accurate and traceable climatological data products derived from different sensors aboard various platforms. While radiometric performances of the OC sensors are independently characterized pre-launch, there is a need for monitoring their stability after lunch and throughout the course of the mission. Short term trends in the instruments' performances are tracked via onboard calibrators, while vicarious and sensor-to-sensor calibrations are carried out for monitoring mid- to long-term trends. A sensor-to-sensor comparison provides clues on whether the differences observed among associated products arise from the differences in the sensors' radiometric performances or from the changes in the bio-optical properties of oceanic waters. This paper examines the relative performance of Aqua-MODIS (MODISA) and Suomi-NPP-VIIRS (SNPP-VIIRS) over the course of 17 months, i.e., March 2012 through July 2013, over ocean waters. The inter-comparison is carried out at the sensor level (L1B), the surface level (L2), and the product level (L3).

The SNPP launched in October 2012 continues the OC mission which began four decades ago with the heritage sensors such as the Coastal Zone Color Scanner (CZCS) followed by the Sea-viewing Wide Field-of-view Sensor (SeaWiFS). The SNPP carries the Visible Infrared Imaging Radiometer Suite (VIIRS), which measures the surface reflected/emitted light in 22 spectral channels with ~370 *m* and ~740 *m* ground sampling distance (GSD) at nadir angles along track[1]. The SNPP is an afternoon satellite (part of the A-Train constellation) [2] placed in a near-circular orbit with an average altitude of 833 *km*. The VIIRS instrument is comprised of a rotating telescope sweeping across track ($\pm$56.26 degrees) covering ~3000 *km* in swath[3]. The optical design of VIIRS includes a half-angle mirror (HAM), which rotates in phase (but at half rate) with the telescope. A combination of rotations of the telescope and the HAM, which minimizes instrument polarization effects, forms the scanning pattern across the swath [4]. Similar to the MODIS design, VIIRS has three focal planes, namely, the visible-near-infrared (VNIR), the short-wave-infrared (SWIR) grouped with the mid-wave-infrared

Earth Observing Systems XVIII, edited by James J. Butler, Xiaoxiong Xiong, Xingfa Gu, Proc. of SPIE
Vol. 8866, 88660J · © 2013 SPIE · CCC code: 0277-786X/13/$18 · doi: 10.1117/12.2023423

(MWIR), and the long-wave-infrared (LWIR). The VNIR focal planes have 16 and 32 detectors laid out along track for moderate resolution (M) and imagery (I) bands, respectively. One of the primary missions of VIIRS is the continuity in providing the science community with the global Environmental Data Records (EDRs) over oceanic waters to enable assessment of climatology, global warming, and net primary production (NPP).

With its life-span far beyond expectations, MODISA has been providing OC products for more than a decade. MODISA performance has been monitored using onboard calibration data, vicarious calibrations, lunar observations, and cross-calibrations with SeaWiFS. The objective behind the in-orbit inter-comparison between SNPP-VIIRS and MODISA is two-folded: a) an early evaluation of the VIIRS instrument relative to MODISA to establish a baseline for temporal trending and b) utilize the baseline difference as a guideline for the future references when MODISA begins to degrade. In addition to characterizing relative in-orbit performance of the two instruments, it is also desired to validate VIIRS-derived OC products relative to those of MODISA. Not only does the surface-level comparison aid in validating the retrieval algorithms (remote sensing reflectance and inherent optical properties), but also it serves as a validation for the in-orbit inter-comparison. In other words, the trends observed for the differences at top-of-atmosphere (TOA) between the two sensors should resemble those found at the surface/product level.

In this paper, we present a trend analysis of the differences between VIIRS and MODIS over a 17-month period. The inter-comparison is made for the TOA level (in-orbit), surface level known as remote sensing reflectance, i.e., R_{rs}, and the inherent optical properties (IOPs), using nearly concurrent MODIS and VIIRS measurements. This analysis complements efforts made by the NOAA STAR/NESDIS, the VIIRS Ocean Science Team (VOST), the OC calibration/validation Team led by NOAA, and the MODIS Characterization Support Team (MCST) at NASA.

2. BACKGROUND

2.1 In-orbit Calibration

Data continuity of the OC products over the global oceans requires instruments with high radiometric fidelity, which satisfies high signal-to-noise ratio (SNR) along with minimal polarization sensitivity, detector-to-detector inconsistencies (banding), and out-of-band responses. The radiometric fidelity of the VIIRS instrument manifests itself in the Sensor Data Record (SDR). The raw data records (RDR), which is referred to as the raw radiometric measurements of the Earth surface, together with the onboard calibration measurements and ancillary data (pre-flight characterizations) are utilized to obtain calibrated radiance imagery termed VIIRS SDR. The VIIRS SDR is the equivalent of the MODIS calibrated radiance (L1B) products in physical units of TOA radiance $[\mathrm{W}/(\mathrm{m}^2\mathrm{sr\ nm})]$.

In addition to the onboard calibration measurements, vicarious calibration (using the observations made at the Marine Optical Buoy (MOBY)) [5] and cross-calibrations are now common-practice [6]. While vicarious calibration is restricted to the number of clear days and the performance of the atmospheric model[7], in-orbit inter-comparisons provide more frequent, near-concurrent observations. Needless to say that the inter-comparison gives insight only into the relative performance of the instruments. Furthermore, for the ocean color calibration/validation, the routine vicarious calibrations over the MOBY site are merely carried out across the blue-green bands. It is critical to monitor an instrument's

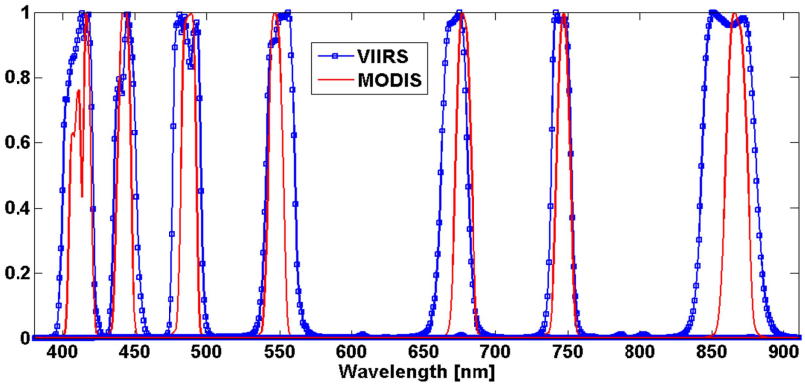

Fig. 1. VIIRS and MODIS VNIR relative spectral response functions (RSRs) associated with the channels applied in this study

Table 1. VIIRS-MODIS channels utilized in this study

	VIIRS		MODIS	
	CW [*nm*]	Bandwidth [*nm*]	CW [*nm*]	Bandwidth [*nm*]
M1	410	20	412	15
M2	443	15	442	10
M3	486	19	488	10
M4	551	19	547	10
M5	671	19	678	10
M6	745	14	747	10
M7	864	38	867	15

radiometric responses in the red and the NIR bands, which are applied in the atmospheric correction procedure[7- 8]. However, it should also be noted that the lunar observations and other onboard calibration activities support monitoring for the NIR channels. Moreover, there are differences in the relative spectral response (RSR) functions of the two sensors that must be accounted for (Fig. 1). Table 1 lists the band configurations associated with VIIRS and MODISA used in this study. Similar to SNPP, Aqua is among the A-train constellation 2, however, it is placed in an orbit with a nominal altitude of 705 *km*. This constellation permits near-simultaneous (< 15 minutes) inter-comparisons between the two imaging sensors onboard, i.e., VIIRS and MODIS. However, for the in-orbit comparisons, the differences in imaging geometries, i.e., scan angle, solar zenith angle, and the orbital altitudes, are unavoidable. Note that the VIIRS spectral channels associated with 740 *m* GSD are referred to as M bands. Although the center wavelengths (CWs) are relatively close (< 4 *nm* shift, except that for M5), the VIIRS spectral bandwidths are broader than those of MODIS (Fig. 1).

2.2 Product Validation

It is also critical to monitor the OC properties derived from the OC missions to ensure fidelity and continuity of ocean color missions. The global monitoring of the OC properties through remote sensing helps to understand global warming patterns, global ocean circulations, ocean clarity, phytoplankton dynamics, coastal/ocean interactions, etc. The remote sensing reflectance, defined as the ratio of water-leaving radiance to downwelling irradiance just above the surface, $(R_{rs}(\lambda), [\, sr^{-1}])$ is the primary variable derived from the TOA radiance collected by the OC sensors. This quantity is critical in the success of an OC mission in that its erroneous retrieval (due to the uncertainties associated with either the imaging device or the atmospheric correction procedure) yields incorrect OC products. It is, therefore, crucial to ensure robust estimations of $R_{rs}(\lambda)$ from which IOPs and chlorophyll-a concentration (CHL) are drawn. This is, in particular, of interest for a long-term, consistent monitoring of ocean properties to study global climate trends.

The inter-comparison between R_{rs} derived from VIIRS and MODIS highlights two aspects: a) validating in-orbit inter-comparisons and b) understanding the discrepancies in the OC higher level products, i.e., IOPs and CHL. Inter-comparisons were conducted for relatively dry upper-air atmospheres with low aerosol loads, where the fidelity of R_{rs} products are usually high. Gordon[9] indicates 1% calibration uncertainty can lead up to 20% error in the retrieved R_{rs}. Making comparisons between the IOPs derived from VIIRS and MODIS aid in identifying the performance of the retrieval algorithms further in the OC processing chain, i.e., the discrepancies observed between R_{rs} products propagate to the IOPs. Monitoring the quality of the OC products not only validates the operations of the relevant algorithms but also it serves as a validating technique for the in-orbit cross-comparisons (TOA) presented in this study (Section 4.2.1).

3. APPROACH

3.1 Top-of-atmosphere (TOA)

For the in-orbit inter-comparisons, the methodology described in a previous study[10] was modified to suit the present study. A preliminary screening of the orbits was performed to choose suitable orbits for a robust inter-comparison. The orbits chosen for inter-comparisons must satisfy the conditions for near-concurrent (< 15 minutes), near-nadir measurements. This criterion restricts selecting VIIRS-MODIS orbit tracks, which closely follow each other (A-train constellation). Note that these orbits differ from simultaneous nadir overpasses defined[11]. Figure 2 illustrates the regions for which the majority of the VIIRS-MODIS inter-comparisons were carried out. In addition to the areas shown in Fig.

2, a few scenes acquired over the Arctic region were also incorporated in the analysis. While the VIIRS SDR scenes were obtained from the Interface Data Processing System (IDPS), the MODIS scenes (Collection 6) were obtained from Level 1 and Atmosphere Archive and Distribution System (LAADS). MODIS scenes were first visually inspected for cloud-free areas along track. When scene candidates were chosen, VIIRS and MODIS scenes were supplied to the processing routine to flag high-quality pixels/areas to estimate the discrepancies between the two sensors at TOA. The search for cloud-free, low aerosol loads, and relatively dry areas is done within the scan range of $\pm 10^{\circ}$ across track. The coefficient of variation (i.e., CV, which represents deviation over mean) for each search window of size 3×3 is calculated for the TOA reflectance at the NIR bands, i.e., $\rho(\mathrm{NIR})$. By setting an appropriate threshold, i.e., CV < 1%, areas of high spatial heterogeneity (due to cloud shadows or aerosols) were avoided. Note that prior to the spatial heterogeneity test, cloud-contaminated pixels and areas with high aerosol loads were masked out. This thresholding leads to flagged areas where candidates are recognized. The temporal consistency in the atmospheric conditions between the overpasses was evaluated by calculating the ratio of $\rho_V(1240)/\rho_M(1240)$, where $\rho_V(1240)$ is the VIIRS M8 channel and $\rho_M(1240)$ represents the MODIS aggregated land band. The subscripts *V* and *M* indicate TOA reflectance associated with VIIRS and MODIS, respectively. The ratio was allowed to vary within $\pm 1\%$ to account for the differences in RSRs. The last step was to choose candidate areas within the scene pairs imaged a) with differences in scan angles less than 5° and b) with similar viewing azimuth angles (both instruments view either east or west when ascending in their orbits). Consequently, the filtered areas (locally averaged) obtained from the two scenes were compared by calculating the percent differences (PD):

$$PD(\lambda)_N = \left(\rho_V(\lambda) - \rho_M(\lambda)\right)/\rho_M(\lambda) \tag{1}$$

where $PD(\lambda)_N$ is expressed in (%). While λ stands for the VNIR bands, i.e., M1–M7, *N* is the number of pixels that PD(λ) are averaged over. In other words, this metric is insensitive to detector-to-detector banding (striping). Note that the number of corresponding areas (*N*) ranged from three to 20 depending on how strictly VIIRS/MODIS scenes were initially masked out.

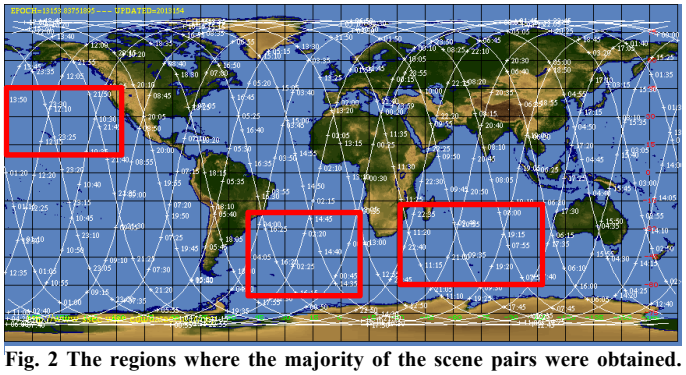

Fig. 2 The regions where the majority of the scene pairs were obtained. The background image shows SNPP orbit tracks (courtesy of the University of Wisconsin, Madison)

Table 2. Configurations for the MODTRAN simulations

	VIIRS	MODIS
Height (km)	$H_1 = 833$	$H_2 = 705$
Scan Angle	α_1	α_2
Upper-air atmosphere	High-latitude Summer	
Aerosol Type	Maritime	
Time	Mean overpass time	
Spectral range/resolution	(400-1000nm)/1nm	
Geographic location	mean lat/long	
Day of year (DOY)	Variable	

The next step is to account for the differences in RSR(λ) and the imaging geometries. This is achieved by creating look-up-tables (LUTs) formed by varying aerosol conditions. The LUT was generated through forward MODTRAN simulations[12] to match $L_V(\lambda)$ and $L_M(\lambda)$, i.e., the measured TOA radiances associated with VIIRS and MODIS, respectively. Table 2 contains MODTRAN configurations for the LUT generation for each scene pair. The TOA radiances $[\mathrm{W}/(\mathrm{m}^2\mathrm{sr\ nm})]$ are then passed through RSR(λ) corresponding to each instrument:

$$L_{eff}(\lambda_0) = \frac{\int_{bandpass} L(\lambda) RSR(\lambda) d\lambda}{\int_{bandpass} RSR(\lambda) d\lambda} \tag{2}$$

where $L_{\mathrm{eff}}(\lambda_0)$ stands for the effective TOA radiance at the center wavelength (λ_0). The match was found by comparing the modeled TOA radiances (resampled to the MODIS RSR(λ)) to those collected by MODIS on a per-band basis (same results would be achieved if comparisons were made for VIIRS). It should be noted that this process aims only at predicting TOA radiances similar to those observed, which leads to estimating the differences due to the discrepancies in

RSR(λ) and imaging geometries, i.e., H and α which stand for altitude and scan angle. The output of this process is a ratio factor (α) found to compensate for such differences:

$$\alpha(\lambda) = \frac{L_V^p(\lambda)}{L_M^p(\lambda)} \quad (3)$$

where $L_V^p(\lambda)$ and $L_M^p(\lambda)$ correspond to the predicted VIIRS and MODIS TOA radiances, which were found to match the observed values. The measured $L_M(\lambda)$ is then adjusted via multiplication by (α), which is then converted to TOA reflectance[13], i.e., $\rho_M(\lambda)$. The adjustment forces the MODIS measurements to appear to have been collected from an identical platform/instrument (SNPP/VIIRS) with the same scan angle and altitude. The (α) parameter found for all the scene pairs ranges from 0.97 to 1.06 depending on the spectral channels and scan angles. A complete description of the uncertainties associated with this adjustment is given in a previous study [10]. Note that the RSRs utilized in this section were the most recent functions characterized through onboard calibration routines. This is, in particular, important for the red and the NIR bands where the signal from oceanic waters is negligible.

3.2 Validation

The approach followed for the comparisons at the surface and IOP levels is similar to that described in Section 3.1. The scene pairs used in the previous section were utilized for VIIRS-MODIS comparisons. Since radiometric uncertainties associated with the instrument, i.e., $\Delta L(\lambda)$, are propagated to the derived $R_{rs}(\lambda)$, this comparison serves as the validation for the in-orbit inter-comparisons (Section 3.1). As a part of the OC calibration/validation activities, it is also desired to analyze the standard VIIRS products processed via IDPS established by the Joint Polar Satellite System (JPSS) at NOAA. The standard atmospheric correction[7] is implemented in IDPS as a primary component of the OC processing scheme. This is followed by the retrieval of the IOPs, including total absorption, a $[m^{-1}]$, and backscattering, $b_b[m^{-1}]$, coefficients, and CHL. The MODIS products, on the other hand, were obtained from the Naval Research Laboratory (NRL). The NRL processing system uses the modified Gordon-Wang model (a broader range of aerosol models are available) to retrieve $R_{rs}(\lambda)$, CHL, IOPs (equivalent of IDPS-processed IOPs)[14], and aerosol radiances.

Similar to the TOA comparisons, here, the cross-comparisons were spatially restricted to the near-nadir angles , i.e., $< \pm 10°$. The MODIS scenes were first searched for areas with minimum local variability (3×3 boxes) and then were masked out by thresholding the local CVs derived from $R_{rs}(410)$ products. The local CV was allowed to reach a maximum of 1%. The $R_{rs}(410)$ products were chosen to restrict the cross-comparisons between spatially uniform oceanic waters to reduce the impact of the differences in the spatial sampling (1km versus 740 m). In a similar fashion, the corresponding areas in the VIIRS products were examined for their variability and, if satisfied, were utilized in the subsequent inter-comparisons. When comparing R_{rs}, the differences in the RSRs should also be taken into account (Eq. 3) due to the (steep) spectral shape of the clear ocean waters. To do so, a typical R_{rs} associated with oceanic waters was run through RSRs to estimate the RSR adjustment factor for different MODIS and VIIRS ocean channels, i.e., M1-M5. After applying the RSR adjustment on the MODIS-derived R_{rs}, the disparity between the two R_{rs} products was computed based on Eq. 1 by replacing the TOA reflectances (ρ) with R_{rs}.

4. RESULTS

A total of 37 scenes over various oceanic/open waters, including the Indian Ocean, South Atlantic, North Pacific, and Southern Ocean (Fig. 2), are included in the analysis for the 17-month period beginning March 1st 2012 (day 61). The diverse set of samples enables a robust relative analysis for the VIIRS-MODIS sensors. The scene pairs are chosen such that at least two data points are available per month. Due to the uncertainties associated with the analysis (particularly in the red-NIR channels), a linear (1×3) averaging filter was applied for all the time series, namely PD_{TOA}, PD_{Rrs}, PD_a, and PD_{bb}, which represent PDs derived for TOA, R_{rs}, total absorption, and backscattering coefficients, respectively. The averaging helps remove small-scale, noisy variability in the time-series.

4.1 In-orbit Trends

The differences in the TOA radiances measured near-simultanous from the two different platforms are presented. Figures 3-4 illustrate the relative trend analysis (Eq. 1) for the ocean channels (410, 443, 486, and 551 *nm*) and the red/NIR bands (671, 746, 862 *nm*), respectively. The y-axis indicates the percent differences (PD_{TOA}) and the x-axis represents days starting from January 1st 2012 as day one. During the early days (day < 120), there is a decreasing pattern seen for $\lambda < 551$ in the relative responses. While the differences for 443 and 486 increase from $< -0.5\%$ to

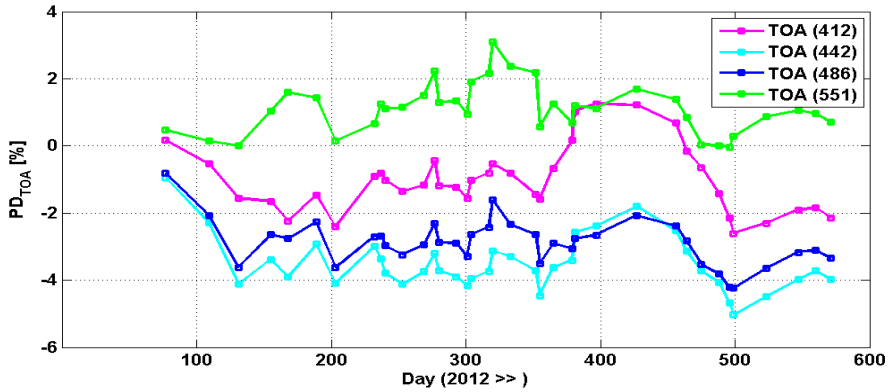

Fig/ 3. The percent difference (PD) trending found for the visible bands at TOA.

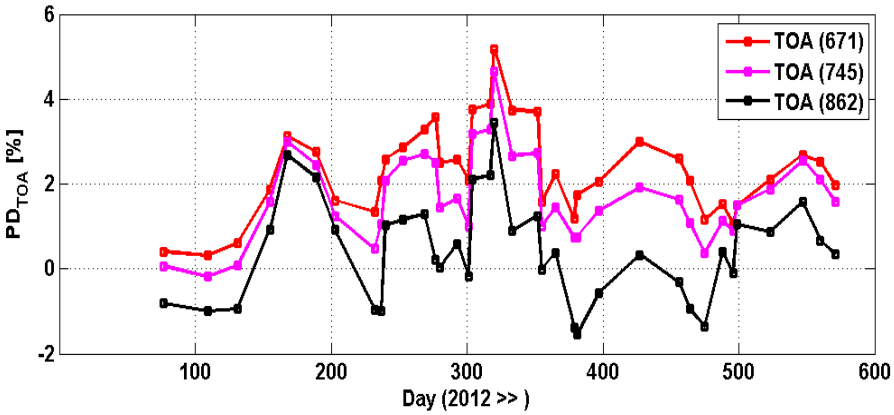

Fig. 4. The percent difference (PD) trending found for the NIR bands at TOA. The trending is less stable than that in the visible bands over the entire period.

$< -3\%$ (VIIRS showing smaller values than MODIS), the trend for $\mathrm{PD_{TOA}}(410)$ rises at the beginning of the year 2013 (reaching a maximum of $+1\%$ in February). This could imply degradation in the MODIS response. The trend in $\mathrm{PD_{TOA}}(412)$ falls to -2.5% in May 2013, i.e., day ~ 500. Note that the depression for day ~ 500 is not observed for M4-M7 (Figs. 3-4). The average relative differences for the entire period for M2 and M3 are -3.3% and -2.7%, respectively. On the other hand, the trend for M1 is found to be within $-2\% < \mathrm{PD_{TOA}} < 0\%$ for the most of the analysis period. The average trend for this channel is -0.85%. The only positive difference among the ocean channels is found for M4, where the temporal average difference is $+1.2\%$. The standard deviations calculated for the spectral trends over the entire timeframe show variability $< +1\%$ for all the ocean channels. After day $= 120$, $PD_{TOA}(410)$ remains relatively flat ($PD_{TOA}(410) = -1.1\%$ until day ~ 350 when it peaks at $+1\%$). The $PD_{TOA}(410)$ temporal variation slowly decreases down to -2.5% at day $= 500$, i.e., early May 2013, followed by a relatively uniform trend (~ -2%, with a slight increase) towards the end of the time series (July 2013). A similar trend is found for other blue bands; however, it is less evident in the green, red, and NIR channels, where the incoming signal is relatively low. The variability for M4 exhibits the lowest ($\sim 0.72\%$), whereas M1 has the highest variability ($\sim 0.9\%$). A relatively larger variability, however, is found for M5-M7 (> 1% for M7), which is attributed to the relatively low signal arising from oceanic waters (within this region) restricting the ability for a robust inter-comparison. The trend analysis for this region is indeed impacted by the temporal inconsistencies in the atmospheric conditions between the acquisitions (even though such inconsistencies were minimized in the filtering chain). The average trend across the entire period for M5, M6, and M7 is found to be $+2.4\%$, $+1.7\%$, and $+0.5\%$, respectively. It should be noted that while these bands have no contributions in the retrieval of OC properties, M6 and M7 are applied in estimating the aerosol optical properties and type. The relatively small disparity between the sensors' NIR responses ensures consistent retrieval of aerosol properties and, as a result, $\mathrm{R_{rs}}$ products. Although majority of the small-scale variability found in the temporal trends corresponds

to the uncertainties associated with the approach[10], changes in the VIIRS/MODIS calibration LUTs yield the large-scale variability (e.g. 360 < day <500 for M1-M3). Note that the inter-comparisons for red/NIR bands are very sensitive to inconsistencies in the atmospheric conditions (between the scene acquisitions) and to the uncertainties associated with estimating the adjustment factor (α)[10].

4.2 Trends in R_{rs} and IOPs

As indicated in Section 3.2, examining consistency between the products derived from VIIRS and MODIS via independent processing chain would a) provide an independent validation for the in-orbit inter-comparisons of the ocean channels (Section 4.1) and b) identify discrepancies in the processing chain. In other words, given all the retrieval processes perform reasonably well, the sensor-to-sensor radiometric differences should propagate to the R_{rs} and then IOP products. This is a valid assumption for the atmospheric correction algorithm, as its performance at near-nadir angles under relatively dry atmosphere with low aerosol load is expected to be high. The relative temporal trends for the R_{rs} products (ocean channels) are illustrated in Fig. 5. By visually comparing trends in R_{rs} with those in Fig. 3, it is found that the overall shape of the trends for the surface-level comparisons resemble those shown for TOA (e.g. a large positive difference within 350 < day < 500 shown for M1 in Fig. 3 and Fig. 5).

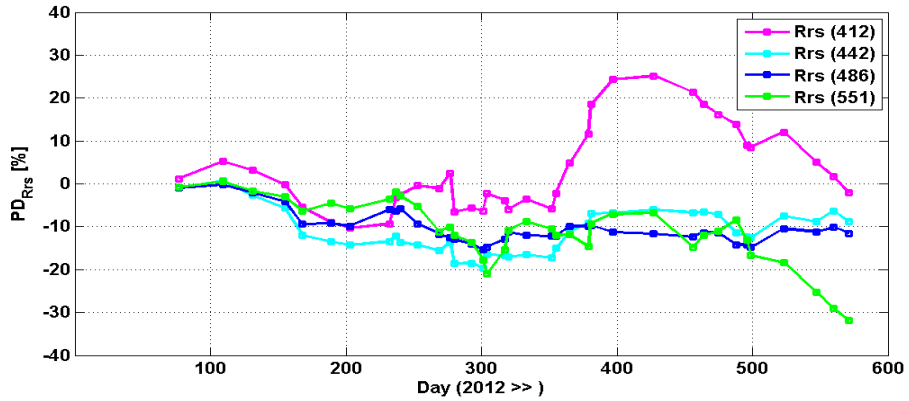

Fig. 5. The PD trending associated with R_{rs}. The temporal variability is consistent with the trends in the TOA study (Fig. 3).

As expected from in-orbit analysis, the difference in $R_{rs}(443)$ is the most negative (on average $\sim -11.4\%$ for day > 120) of all ocean bands, whereas the relative difference for M1 was found $\sim +3.9\%$. It is also found that a relatively small positive or negative differences at TOA may not lead to a positive or negative difference in R_{rs}. This is evident from the temporal patterns seen for M4 where the temporal PD_{Rrs} is positive ($0\% < PD_{Rrs} < +2.2\%$) for the entire timeframe when analyzing in-orbit radiance observations. The $PD_{Rrs}(551)$ > 0% prior to day = 220 and then slowly plateaus at -10%. The decrease in $PD_{TOA}(551)$ is also evident for day > 350 for which the mean difference is $+0.9\%$. This unexpected bias with a reverse sign may come from two sources, namely inconsistencies in R_{rs} retrieval due to small differences in the NIR bands (Fig. 4) and/or extremely low water-leaving radiance at $551\ nm$, i.e., small errors in the retrieval processes may cause large uncertainties in R_{rs}. Similar trends are found for the blue channels during day < 120 ($PD_{Rrs}\sim 15\%$ while $PD_{TOA} = 0\%$). Although positive differences for $PD_{TOA}(671)$ were also obtained, $PD_{Rrs}(671)$ (not shown here) was found to be, on average, $\sim -45\%$ for the entire timeframe. This can be well attributed to the different signal-to-noise ratio of the two sensors and an imperfect atmospheric correction for such a small water-leaving signal, i.e., $R_{rs}(671) \approx 2e^{-4}\ [1/sr]$.

The IOPs including the total absorption (a) and backscattering (b_b) are examined to characterize the relative performance of the retrieval algorithms[14] when applied on VIIRS and MODIS datasets. Since R_{rs} is proportional to b_b/a, the trend observed in PD_{Rrs} is expected to propagate to PD_a and PD_{bb}. Figures 6-7 show the relative temporal trend over the 17-month period. While PD_a exhibits significant local irregularities in the time series (3.5 ×, on average, larger than that of PD_{Rrs}), PD_{bb} shows smoother trends (for all ocean channels) where only large-scale trends are notable. The mean temporal trend for the absorption is $+1.3\%$, $+11.2\%$, $+7.4\%$, and $+9.5\%$ for M1-M4 bands, respectively.

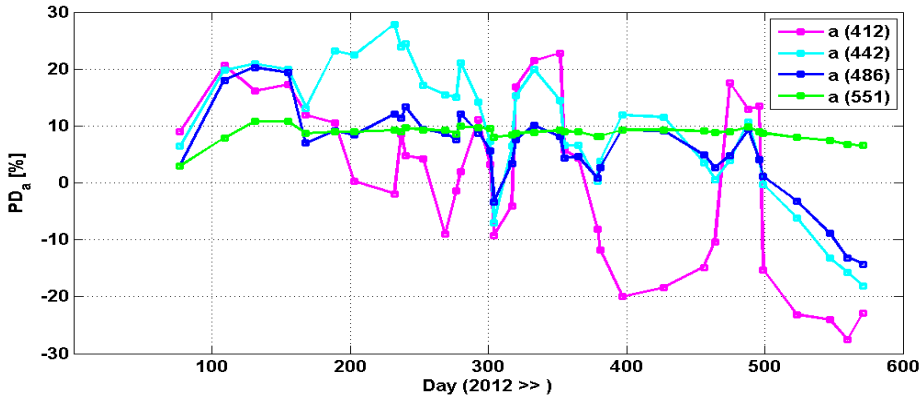

Fig. 6. The PD trending associated with absorption (*a*) properties (M1-M4) of oceanic waters

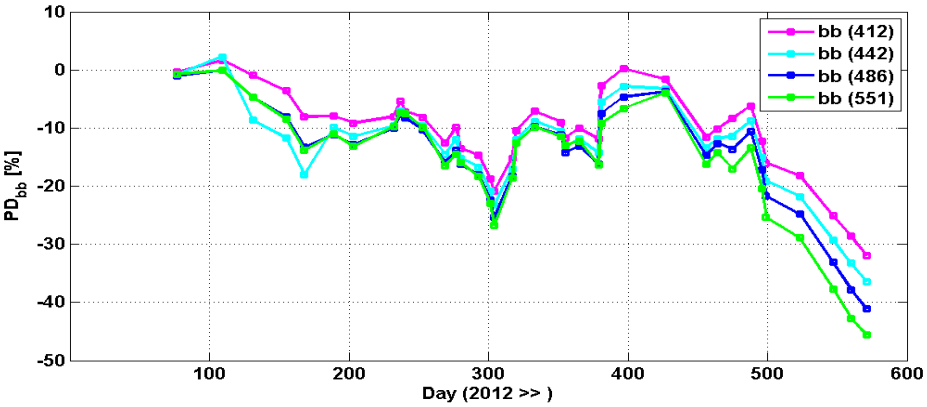

Fig. 7. The PD trending associated with the backscattering (b_b) properties (M1-M4) of oceanic waters

The discrepancies for PD_{bb} is found to be -11%, -14%, -15%, and -16%, respectively. The trend in PD_{bb} for all the ocean channels (Fig. 7) closely resembles those for PD_{Rrs}, whereas PD_a for M2-M4 are the only trends correlated ($r \sim 0.6$) with the corresponding PD_{Rrs} trends (Fig. 5). The exception is $PD_a(410)$ where the correlation with the corresponding $PD_{Rrs}(410)$ is very weak ($r < 0.08$). This is due to the significant variability found for $PD_a(410)$, i.e., a is very sensitive to small variability in R_{rs}. On the other hand, although $PD_{bb}(410) < 0$ for the entire period, $PD_{Rrs}(410) > 0$ for day > 360. This is attributed to the fact that R_{rs} is inversely related to the total absorption ($R_{rs} \approx b_b/a$), then a positive PD_{Rrs} will transfer negative PD_a (Fig. 6) where b_b is, in general, proportional to R_{rs} in the green band[14].

5. CONCLUSIONS

In this paper, the VIIRS-derived products over the oceans, including SDR and EDR, were compared against the corresponding products obtained from MODIS for the period of March 2012 through July 2013. The in-orbit inter-comparison between the two instruments indicates a relative consistency in the short visible bands for DOY< 120. However, the consistency decreases after DOY=120. The average difference for 2012 was found to be -1.1%, -3.5%, -2.8%, and $+1.3\%$ for the M1-M4 channels, respectively. The average difference gradually decreases in 2013 (January through July) reaching to -1.8%, -3.8%, -3.2%, and $+1.1\%$, respectively. The differences in the red/NIR bands (M5-M7) were found to be relatively stable, i.e., $+2.6\%$, $+1.9\%$, and $+0.7\%$, over the entire timeframe. Such disparities at the TOA level yields -3.3%, -14.6%, -10.1%, and -8.7% differences in R_{rs} for M1-M4, respectively, during 2012.

The shapes for the temporal trends at the TOA level and surface level were found consistent. As expected the anomalies seen in R_{rs} are propagated in the total absorption and backscattering coefficients.

6. ACKNOWLEGEMENTS

The authors would like to thank the ocean color calibration/validation team for providing comments/feedback on the progress of this study. We also would like to appreciate the help from Sherwin Ladner with NRL. Financial support provided by NOAA STAR program is greatly appreciated.

REFERENCES

[1] Raytheon Company "NPOESS Visible Infrared Imaging Radiometer Suite (VIIRS) Sensor Design and Performance,"2003, http://cimss.ssec.wisc.edu/itwg/itsc/itsc13/session10/Puschell%20VIIRS%20Sensor%20Performance%20ITSC%20FINAL.pdf
[2] NASA,"Introducing the A-Train,"2010, http://www.nasa.gov/mission_pages/a-train/a-train.html
[3] Wu, A. and Xiong, X.,"NPP VIIRS and Aqua MODIS RSB comparison using observations from simultaneous nadir overpasses (SNO),"85100P-85100P (2012).
[4] Hammann, M. G. and Puschell, J. J.,"SeaWiFS-2: an ocean color data continuity mission to address climate change,"745804-745804 (2009).
[5] Franz, B. A., Bailey, S. W., Werdell, P. J. and Mcclain, C. R.,"Sensor-independent approach to the vicarious calibration of satellite ocean color radiometry,"Appl. Opt., 22(46), 5068-5082 (2007).
[6] Kwiatkowska, E. J., Franz, B. A., Meister, G., Mcclain, C. R. and Xiong, X. X.,"Cross calibration of ocean-color bands from Moderate Resolution Imaging Spectroradiometer on Terra platform,"Applied Optics, 36(47), 6796-6810 (2008).
[7] Gordon, H. R. and Wang, M.,"Retrieval of water-leaving radiance and aerosol optical thickness over the oceans with SeaWiFS: a preliminary algorithm,"Appl. Opt., 3(33), 443-452 (1994).
[8] Wang, M. and Gordon, H. R.,"Calibration of ocean color scanners: how much error is acceptable in the near infrared?,"Remote Sensing of Environment, 2–3(82), 497-504 (2002).
[9] Gordon, H. R.,"Radiometric considerations for ocean color remote sensors,"Applied Optics, 22(29), 3228-3236 (1990).
[10] Pahlevan, N. and Schott, J. R.,"Characterizing the relative calibration of Landsat-7 (ETM+) visible bands with Terra (MODIS) over clear waters: The implications for monitoring water resources,"Remote Sensing of Environment, 125), 167-180 (2012).
[11] Cao, C., Weinreb, M. and Xu, H.,"Predicting Simultaneous Nadir Overpasses among Polar-Orbiting Meteorological Satellites for the Intersatellite Calibration of Radiometers,"Journal of Atmospheric and Oceanic Technology, 4(21), 537-542 (2004).
[12] Berk, A., Bernstein, L. and Robertson, D. C., Spectral Sciences,"MODTRAN: a moderate resolution model for LOWTRAN 7,"GL-TR-89-0122(1989.
[13] Schott, J. R., [Remote Sensing The Image Chain Approach], Oxford Unversity Press, New York 666 (2007).
[14] Carder, L., Chen, R., F., Lee, Z., Ping, Hawes, S. K. and Cannizaro, J., P., University of South Florida "MODIS Ocean Science Team Algorithm Theoretical Basis Document,"67, 2003.